Mathieu Colin de Verdiere, Anthony K. Pickett, Alex A. Skordos, Volker Witzel

1 INTRODUCTION

Efficient design and manufacturing processes are key elements of successful composites production. End users of composite materials in various industrial sectors such as aerospace, automotive and marine focus on structural composites that can provide a beneficial combination of in-plane and out-of-plane mechanical performance with impact resistance, whilst satisfying criteria and constraints related to weight, cost and robustness of the final component. The use of non crimped fabric (NCF) composites in the context of liquid composite moulding allows fast processing as several layers of reinforcement can be placed in the mould in a single step, before infusion under flexible or rigid tooling. This potential improvement in process speed is combined with advanced in-plane properties resulting from the absence of crimp in NCFs.

As with any other class of continuous fibre/thermosetting matrix composites the superior in-plane performance of NCFs is accompanied by susceptibility to delamination. A number of methodologies have been developed to address this issue focusing on the use of toughened resin systems, on 3D weaving/braiding and on through thickness reinforcement. The latter reinforces the interface between plies and partially locks adjacent layers of the laminate using a small amount of fibres oriented in the thickness direction. Various techniques have been employed to achieve this, including stitching, z-pinning and tufting.

In stitching a needle is used to perforate the fabric and to insert a high strength yarn which is locked by a second thread. Stitching affects delamination properties positively with notable improvements in both mode I and mode II toughness [1-3]. In-plane mechanical behaviour is also influenced with potential improvement or degradation of properties depending on laminate type, manufacturing route, stitching condition and loading type [4]. Stitching also enhances the impact response of laminates with significant improvements under impact conditions that favour the formation of large delaminations [5]. The final set of properties obtained is influenced to a large extend by damage, such as resin pockets, broken fibres and fibre kinking and misalignment, introduced during stitching [4, 6].

In z-pinning pultruded carbon pins contained in crushable foam are inserted in pre-impregnated textiles using an ultrasonic hammer. The insertion of z-pins improves significantly the delamination response of composite laminates [7, 8]. Similarly to stitching z-pinning induces crimping and distortion of fibres as well as resin rich pockets which degrade the in-plane response of laminates [9, 10].

Tufting is performed using a hollow needle that carries the tuft through a dry fabric and retracts, allowing the action of friction to constraint the through-the-thickness thread. Compared to stitching, tufting is a simpler process which induces less damage to the fabric as a result of the lower tension applied to tufting threads. Tufting increases the load carrying capacity of structures prone to delamination damage [11] and improves both the delamination [12] and compression after impact response of laminates [6].

In this study the behaviour of tufted and untufted carbon/epoxy NCF composites produced using resin infusion is investigated in tension, compression, cyclic shear and mode I and II delamination. A finite element model of the mechanical response of tufted and untufted composites is developed based on the use of composite shell elements that incorporate non-linear and failure in-plane behaviour and modelling of delamination via a cohesive interface. Model verification and validation is performed using the results of coupon testing.

Mathieu Colin de Verdiere, Anthony K. Pickett, Alex A. Skordos, Volker Witzel

2 MATERIALS AND EXPERIMENTAL TECHNIQUES

2.1 Specimen fabrication

The material used in this study was an NCF carbon/epoxy composite. The carbon fibres used were HTA 6 K from Tenax aligned by Saertex in a bidiagonal ($\pm$ 45°) carbon non crimp fabric with an areal density of 540g/m^2. Tufted specimens were produced using HTA 1k Tenax thread. A 5 mm $\times$ 5 mm pattern was used and tufting was aligned to the 0° direction of the NCF material. Panels with dimensions of 700 mm $\times$ 300 mm and layup sequences of [0/90]$_3$ or [0/90]$_4$ were infused under vacuum at 120 ^{o}C. The epoxy resin used was RTM6 (Hexcel). After completion of filling the material was cured at 160 ^{o}C for 3 hours. Panels for delamination tests incorporated a 60 mm wide 13 μm thick PTFE film inserted along the length of the panels at mid-thickness. Aluminium tabs were bonded to specimens used for in-plane experiments and steel blocks were attached to delamination specimens. The specimens lay up, size and tabs for the various tests are summarised in table 1.

Test	Layup	Dimensions(mm)	Tabs (mm)
Compression – untufted	[0/90]$_{3s}$	80$\times$25$\times$3.3	13$\times$25$\times$1.5
Cycling compression [$\pm$45] – untufted	[$\pm$45]$_{3s}$	80$\times$25$\times$3.3	13$\times$25$\times$1.5
Tension- untufted	[0/90]$_{3s}$	250$\times$25$\times$3.3	50$\times$25$\times$1.5
Cycling tension [$\pm$45] – untufted	[$\pm$45]$_{3s}$	250$\times$25$\times$3.3	50$\times$25$\times$1.5
Compression- tufted	[0/90]$_{4s}$	80$\times$25$\times$4.4	13$\times$25$\times$1.5
Cycling compression [$\pm$45] – tufted	[$\pm$45]$_{4s}$	80$\times$25$\times$4.4	13$\times$25$\times$1.5
Tension- tufted	[0/90]$_{4s}$	250$\times$25$\times$4.4	50$\times$25$\times$1.5
Cycling tension [$\pm$45] – tufted	[$\pm$45] $_{4s}$	250$\times$25$\times$4.4	50$\times$25$\times$1.5
Delamination Mode I double cantilever beam	[90/0]$_{4s}$	200$\times$20$\times$4.4	20$\times$20$\times$10
Delamination Mode II end loaded specimen	[90/0]$_{4s}$	200$\times$20$\times$4.4	20$\times$20$\times$10

Table 1: Geometry and layup of specimens.

2.2 In plane testing

Tension tests were carried out on an Instron testing machine with a 100 kN load cell. The loading speed was 0.7 mm/min for axial tension tests and 1.5 mm/min for cyclic [$\pm$45] tests. Compression testing was carried out using the set up shown in Fig. 1.a which was designed for use with the optical strain field recording system illustrated in Fig. 1.b. Compression specimens were loaded via their top end while a cap was added to prevent delamination of the composite. Steel anti-buckling guides of dimensions 3$\times$5$\times$50 mm were inserted in the gaps of the test fixture to allow the use of long gauge length specimens in compression.

A LIMESS optical strain measurement system allowed the recording of the three dimensional displacement field over a wide area of the tension and compression specimens. The system uses two cameras whilst a sprayed pattern allows an image analysis algorithm based on image correlation to estimate the displacement vector of each point over two sequential frames. Execution of a calibration procedure as well spraying of an appropriate pattern and suitable lighting conditions are required for successful use of the system.

| (a) Test fixture | (b) Optical strain measurement set up |

Figure 1: Compression test.

2.3 Delamination testing

Delamination tests were carried out on a Zwick test machine equipped with a 2 kN load cell. Mode I double cantilever beam delamination tests followed the ASTM D 5528 protocol [13]. The loading speed was 3 mm/min and the crack interface was located between 0° plies. One specimen side was painted and marked every 2 mm. to permit monitoring and recording of the crack length as a function of time. Simultaneous recording of load and crosshead displacement allowed the calculation of strain energy release rate [14]. Mode II end loaded specimen tests were carried out following the ELS protocol analysis developed by the ESIS TC committee [15]. Similarly to mode I testing the crack interface was located between 0° plies and crack length, load and displacement were recorded. The strain release energy in shear was calculated according to the procedure outlined in [15].

3 MODELLING

The mechanical behaviour of tufted and untufted laminates is simulated using a finite element model. The model combines composite shell elements with non-linear behaviour incorporating in-plane damage and cohesive interface elements that simulate delamination damage. The model is implemented in the explicit finite element code PAM-CRASH [16] following the procedures proposed by Pickett et al. [17-19].

3.1 In-plane damage model

The explicit finite element code used implements the Ladeveze and Le Dantec damage model [20] in a multi-layered thin shell element [16]. This model represents each ply in the laminate via an elastic-plastic stress strain relationship which also incorporates damage.

$$\{\boldsymbol{\sigma}\} = [\mathbf{C}]\{\boldsymbol{\varepsilon}\} \tag{1}$$

Where $\{\boldsymbol{\sigma}\} = (\sigma_{11}, \sigma_{22}, \sigma_{12}, \sigma_{23}, \sigma_{31})^T$ is the stress vector, $\{\boldsymbol{\varepsilon}\} = (\varepsilon_{11}, \varepsilon_{22}, \varepsilon_{12}, \varepsilon_{23}, \varepsilon_{31})^T$ the strain vector and $[\mathbf{C}]$ the non-linear compliance tensor expressed as follows,

$$[\mathbf{C}] = \begin{bmatrix} \dfrac{E_{11}}{1-v_{21}v_{12}} & \dfrac{v_{21}E_{11}}{1-v_{21}v_{12}} & 0 & 0 & 0 \\ \dfrac{v_{21}E_{11}}{1-v_{21}v_{12}} & \dfrac{E_{22}}{1-v_{21}v_{12}} & 0 & 0 & 0 \\ 0 & 0 & G_{12}(1-d_{12}) & 0 & 0 \\ 0 & 0 & 0 & G_{23}(1-d_{12}) & 0 \\ 0 & 0 & 0 & 0 & G_{12}(1-d_{12}) \end{bmatrix} \qquad (2)$$

Here subscript 1 denotes the fibre direction of the ply, E_{11} and E_{22} are moduli in the fibre and transverse direction respectively and G_{12}, G_{23} are shear moduli. The damage factor d_{12} is a function of the stress/strain path followed [18] and introduces non-linearity in the model. The parameters required for calculation of the evolution of the damage factor are estimated from cyclic experiments. The present implementation for non crimped fabric does not require use of damage factors for moduli in the fibre or transverse direction. A dependence of axial moduli on the strain can be considered, whereas failure is modelled via the use of an ultimate strain over which the corresponding modulus vanishes.

3.2 Delamination model

Delamination damage is modelled using an interface which applies a force-displacement law between corresponding nodes of adjacent layers of the laminate. Components related to normal and tangential displacement along the interface are used to represented mode I and II delamination damage respectively. The force-displacement curve follows the general shape illustrated in Fig. 2 for both mode I and mode II delamination. The behaviour of the interface is elastic up to a maximum force after which damage occurs.
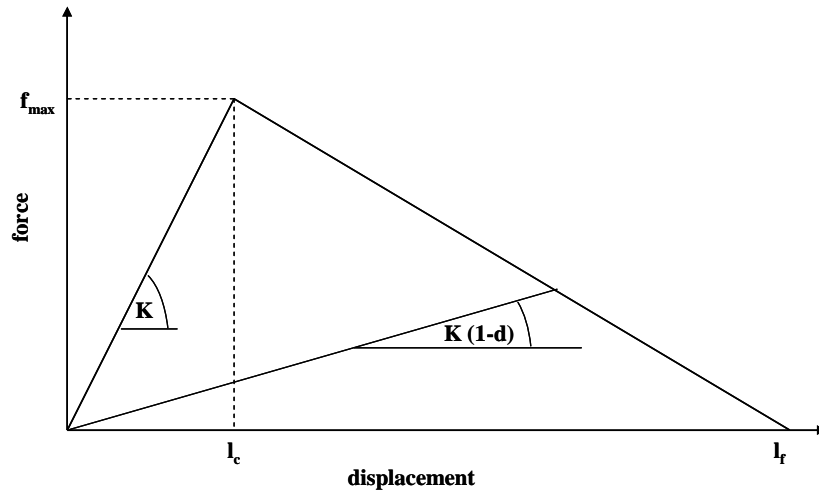

Figure 2: Force-displacement curve of the cohesive interface

The area under the force-displacement curve corresponds to delamination toughness (G_{IC} or G_{IIC}) The stiffness of the interfacial link K is reduced due to damage to $K(1-d)$ with factor d depending on accumulated damage as follows,

5

$$d = \begin{cases} \dfrac{l - l_f}{l_c - l_f}, & l > l_c \\ 0, & l \le l_c \end{cases} \tag{3}$$

In mixed mode loading conditions modes I and II need to be coupled. Linear coupling is used in the present model for this purpose [18].

3.3 Model implementation

Finite element models of the compression, tension and delamination tested were implemented in PAM-CRASH. The model uses shells to simulate the inplane elastic and damage behaviour of laminates and interfacial links to represent delamination damage. Tufts are represented by links that follow a linear behaviour until failure. The failure is governed by a limit load which is independently defined for the shear and normal components of the link.

Tension specimens were represented by a layer of 320 shell elements and compression specimens by a layer of 180 shells. Uniaxial boundary conditions were applied, whilst in the case of the compression model additional out of plane constraints were used to represent the antibuckling guides. The dimensions and layups of the models are identical to those given in Table 1.

Delamination models (Fig. 3) comprised two layers of shell elements (320 elements per layer) each of them representing half of the layup. The two halves were disconnected in the area of the pre-crack film and connected by interfacial links in the rest of their common surface, while contact was applied between the two shells to avoid penetration. Mode I models were constrained at the end tip of the DCB with opposite prescribed displacements applied to each side of the DCB loading end. Mode II models were constrained at locations that are clamped during and ELS test with a prescribed displacement was applied to one side of the free end of the specimen.
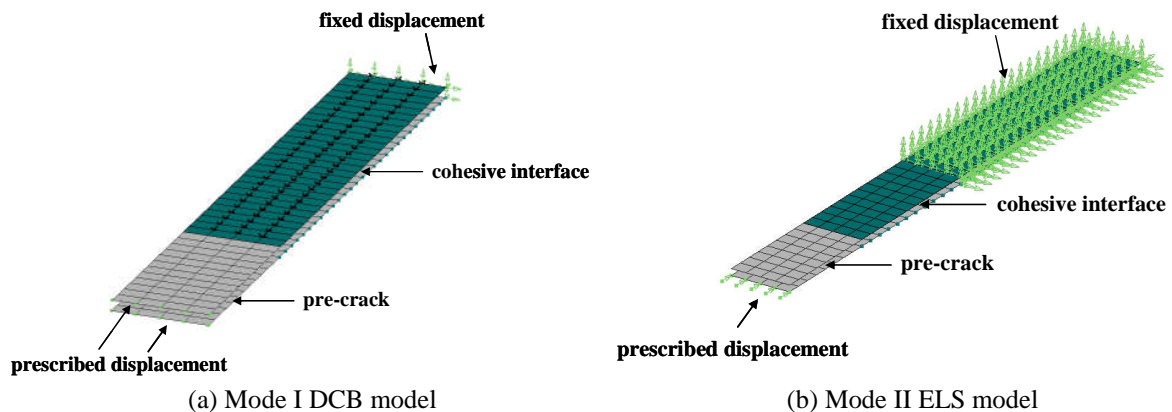

(a) Mode I DCB model   (b) Mode II ELS model

Figure 3: Delamination models.

4 RESULTS AND DISCUSSION

4.1 In plane response

Fig. 4 illustrates the results of axial tension and compression experiments. Table 2 summarises the major material parameters obtained in these experiments and used to estimated material properties for subsequent modelling. It can be observed that tufting reduces the in plane stiffness of the material from 63 to 55 GPa due to a "dilution" effect. Failure strains are simi-

6

lar for tufted and untufted NCF composites in both tension and compression while failure stress decreases by about 10-15 % with tufting. Non linearity is more apparent in tufted specimens. Comparison of the tension and compression behaviour indicates significant variations induced by the domination of different failure mechanisms, such as micro-buckling in compression and fibre fracture in tension. Strength and ultimate strains are significantly lower in compression whilst non linearity tends to be more pronounced in compression than in tension.
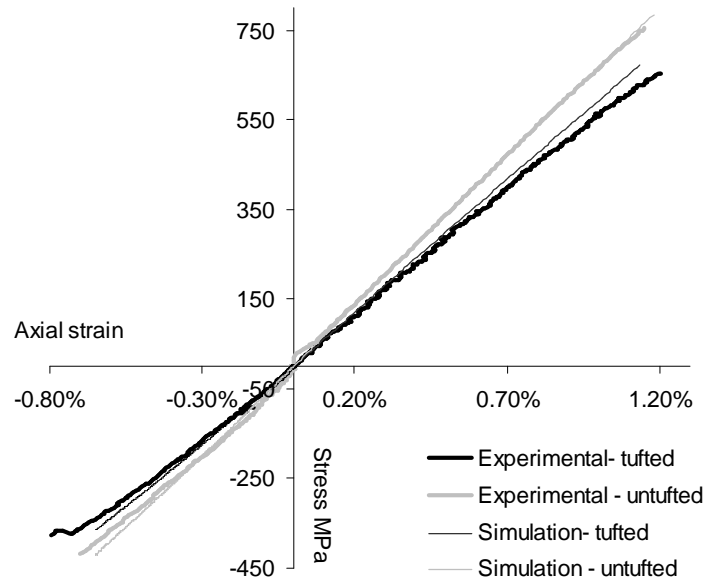

Figure 4: Axial tension and compression experimental and simulation behaviour of tufted and untufted NCF composites.

	Untufted	Tufted
Tensile modulus (GPa)	63	55
Tensile ultimate strain (%)	1.26	1.20
Tensile strength (MPa)	755	654
Compressive modulus (GPa)	63	56
Compressive ultimate strain (%)	0.70	0.71
Compressive strength (MPa)	418	374

Table 2: Material parameters obtained from axial tension and compression tests of NCF composites.

The finite element model results are compared with the experimental response in Fig. 4. It can be seen that the model follows the experimental behaviour closely with respect to both stiffness and strength of coupon specimens. These results are mostly a verification of the implementation of the model and not of its predictive capabilities as the experimental curves are directly related to the material properties used in the models.

The cyclic behaviour of [±45] NCF composites under tension and compression is illustrated in Fig. 5. The shear tensile response of untufted and tufted material is similar in terms of initial shear modulus, failure strain, strength, and plasticity. The strength of the tufted composite is slightly higher with higher plastic strains in compression than in tension, while the untufted material also shows higher strains without the corresponding increase in strength.

The untufted material showed more plasticity in compression than in tension but no added strength. Table 3 summarises the material data obtained in the cyclic experiments.
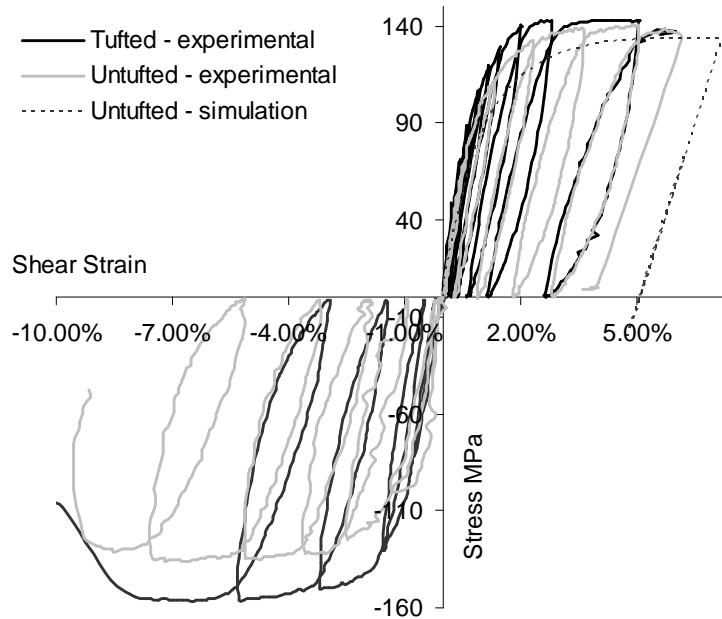

Figure 5: Cyclic $[\pm 45]$ tension and compression experimental and simulation behaviour of tufted and untufted NCF composites.

	Untufted	Tufted
Initial tensile shear modulus (GPa)	6.6	7.4
Tensile ultimate strain (%)	6.25	6.09
Tensile strength (MPa)	139	143
Initial compressive shear modulus (GPa)	8.0	7.6
Compressive ultimate strain (%)	> 8.7	> 8.1
Compressive strength (MPa)	135	156

Table 3: Material parameters obtained from shear tension and compression tests of NCF composites

Damage was estimated as the reduction in modulus during cyclic tests over the surface of the specimens. Figs. 6-9 illustrate the damage field for the various test cases. There are significant differences in behaviour between tufted and untufted laminates and between loading in tension and in compression. As it can be observed in Fig. 6 there is a close correspondence between the damage field calculated using optical strain measurements and the results of ultrasonic C-scan. The damage field in the untufted laminate indicates non-uniformity across both the length and the width of the specimen (Fig. 5). In contrast, compressive damage tends to be distributed uniformly across the width of specimens with tufts (Fig. 6). The untufted material undergoes large local shear deformation that leads to separation (Fig. 8(b)).
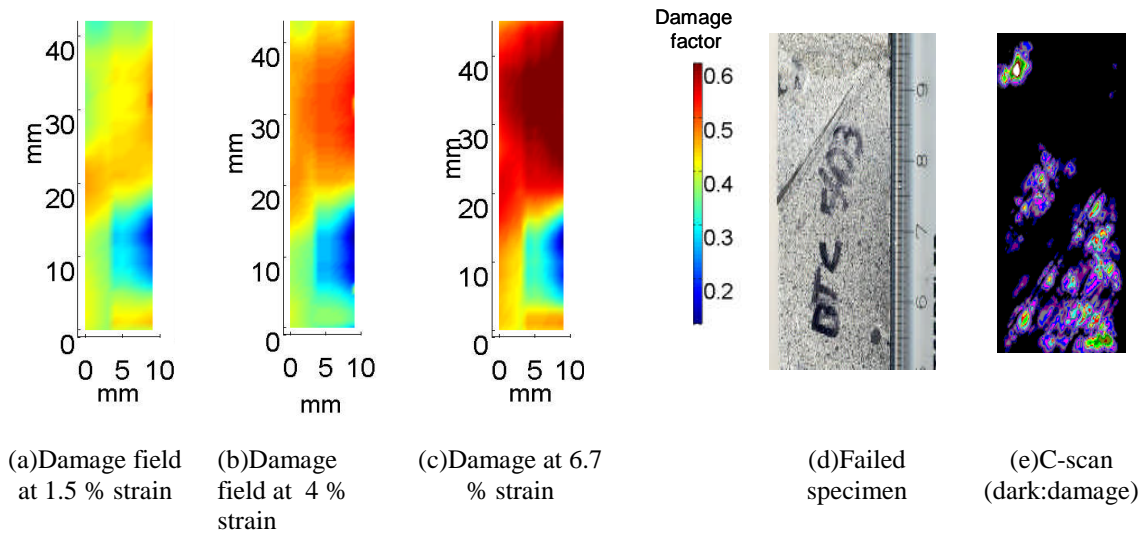
(a)Damage field at 1.5 % strain   (b)Damage field at 4 % strain   (c)Damage at 6.7 % strain   (d)Failed specimen   (e)C-scan (dark:damage)
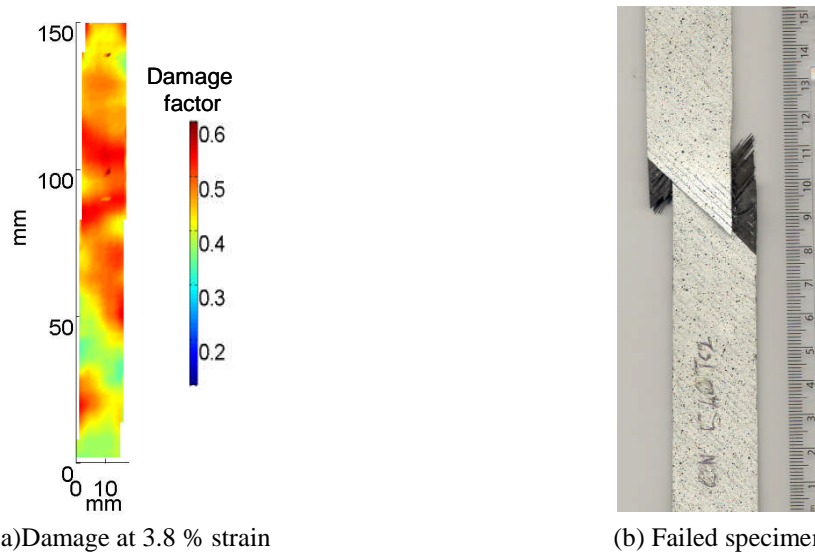
Figure 6: Damage field evolution, specimen and C-scan of the untufted specimen in compression

(a)Damage field at 0.75 % strain   (b)Damage field at 2 % strain   (c)Damage at 4 % strain   (d)Failed specimen   (e)C-scan (dark:damage)
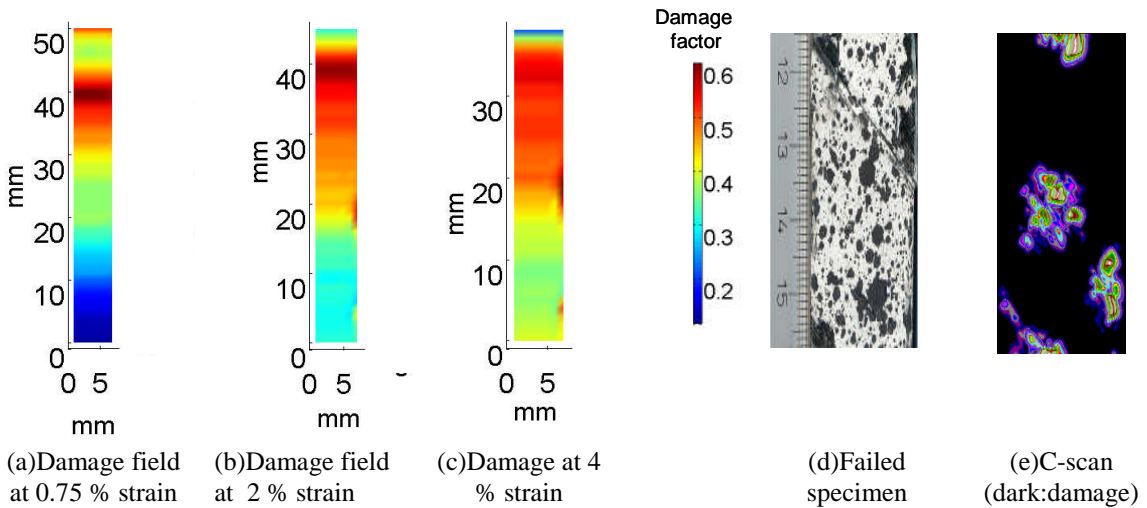
Figure 7 Damage field evolution, specimen and C-scan of the untufted specimen in compression

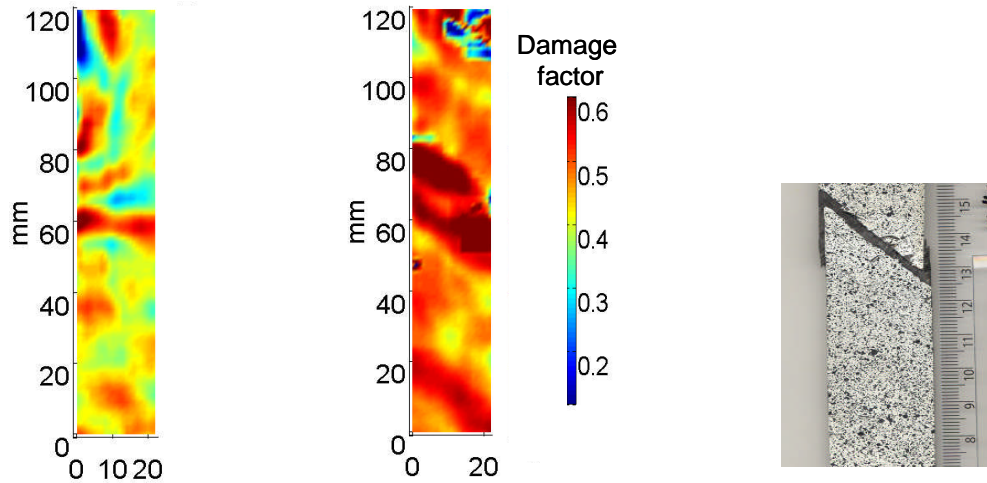(a)Damage at 3.8 % strain   (b) Failed specimen

Figure 8: Damage field evolution, specimen and C-scan of the untufted specimen in tension

(a)Damage field at 0.75 % strain   (b)Damage field at 2 % strain   (c) Failed specimen

Figure 9: Damage field evolution, specimen and C-scan of the tufted specimen in tension

4.2   Delamination

The results of delamination experiments are illustrated in Fig. 10. In mode I the untufted laminate shows stable crack propagation. In contrast, the results for tufted specimens indicated unstable crack growth, while delamination accompanied by a three-fold increase in maximum load. In mode II the maximum load reached is similar for the untufted and the tufted material. However, crack propagation occurs with a significant reduction in load in the monolithic laminate whilst the load remains at an almost constant level during crack propagation in the tufted material.
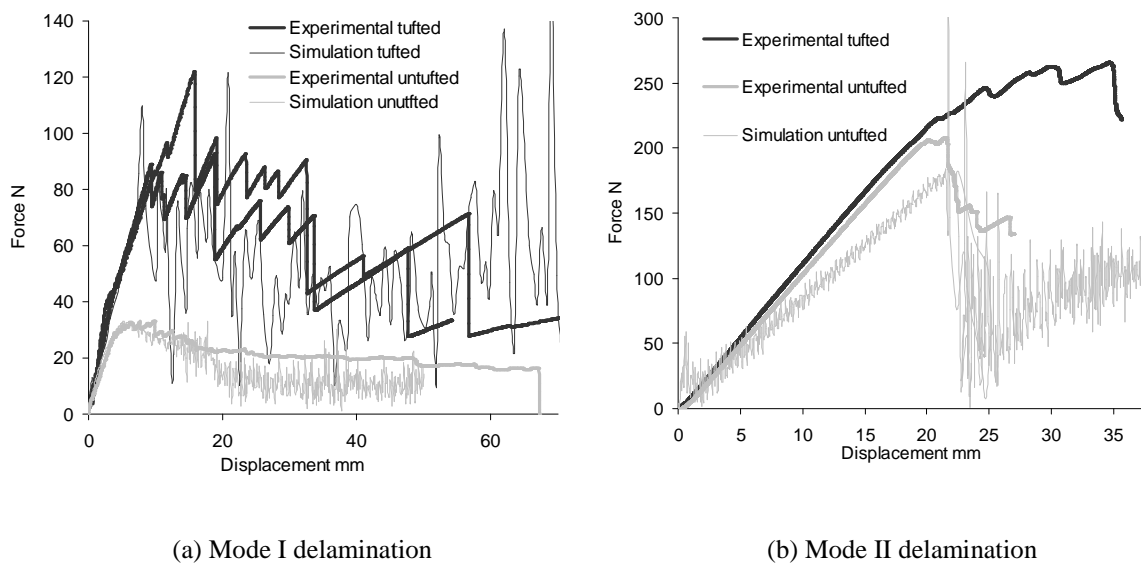
(a) Mode I delamination   (b) Mode II delamination

Figure 10: Results of delamination testing and simulation.

Mathieu Colin de Verdiere, Anthony K. Pickett, Alex A. Skordos, Volker Witzel

Material parameters extracted from these experiments and used for mode I and II coupon simulation are summarised in Table 4. A comparison of model and experimental results is shown in Fig. 10. It can be observed that mode I results are reproduced closely by the model. Similarly, mode II results are reproduced successfully in the case of the untufted material. Lower apparent stiffness of the model response is related to slight discrepancies between model and experiment in the load application. An estimation of the tuft strength under mode II was not possible as it was not possible to estimate displacement at the initial pre-crack tip form load displacement data. In the case of mode I this is easily carried out using a non-linear elastic solution for the beam.

	Mode I	Mode II
Interface modulus (GPa)	2.9	2.9
Initiation stress (MPa)	0.8	35.0
Strain energy release rate (J/m^2)	429	1200
Tuft link strength (MPa)	270	-

Table 4: Material parameters obtained from delamination tests.

5 CONCLUDING REMARKS

This study focused on the enhancement of the mechanical behaviour of non crimped fabric composites by tufting. Experimental studies on the in-plane and delamination response were carried out and a finite element model incorporating non-linearity in the in-plane response and delamination damage was developed.

The in-plane response of both tufted and untufted laminates was found to be non-linear, while tufting reduced the modulus and strength of laminates by 10-15%. The response of [±45] non crimped fabrics was different in compression and tension with significantly higher strain to failure in compressive conditions. Similarly, the influence of tufting was more significant in compression. Cyclic loading enabled the estimation of damage distributions under [±45] loading. Ultrasonic C-scans validated successfully this analysis which indicated that tufting results in more uniform damage distribution in the normal to the load direction. Delamination resistance increased significantly with tufting. Tufted specimens reached higher loads under mode I, whilst crack propagation occurred without load reduction in mode II.

The model implementation was verified against the results of coupon testing. The non-linear response of both tufted and untufted specimens was reproduced successfully. Delamination damage behaviour was followed closely by the model and the concept of modelling the tufts as a series of links yielded good results in mode I. These results constitute mainly a verification of the model implementation. Model validation using loading conditions independent of those followed in testing for parameter estimation will be performed in the future to provide an evaluation of the predictive capabilities of the simulation.

REFERENCES

[1] K. A. Dransfield, L. K. Jain, Yiu-Wing Mai, On the effect of stitching in CFRPs-I modeI delamination toughness. *Composites Science and Technology,* **58**, 815-827, 1998.

[2] L. K. Jain, K. A. Dransfield, Yiu-Wing Mai, On the effect of stitching in CFRPs-II modeII delamination toughness. *Composites Science and Technology*, **58**, 829-837, 1998.

[3] R. Velmurugan, S. Solaimurugan, Improvements in Mode I interlaminar fracture toughness and in-plane mechanical properties of stitched glass/polyester composites. *Composites Science and Technology*, **67**, 61–69, 2007.

[4] A. P. Mouritz, K. H. Leong and I. Herszberg, A review of the effect of stitching on the in-plane mechanical properties of fibre-reinforced polymer composites. *Composites Part A: Applied Science and Manufacturing,* **28A**, 979-99 I, 1997.

[5] F. Aymerich, C. Pani, P. Priolo, Damage response of stitched cross-ply laminates under impact loadings. *Engineering Fracture Mechanics,* **74,** 500–514, 2007.

[6] C. Scarponi, A. M. Perillo, L. Cutillo, C. Foglio, Advanced TTT composite materials for aeronautical purposes: Compression after impact (CAI) behaviour. *Composites: Part B,* **38**, 258–264, 2007.

[7] I. K. Partridge, D. D. R. Cartié, Delamination resistance laminates by Z-Fiber pinning: Part I manufacture and fracture performance. *Composites Part A: Applied Science and Manufacturing,* **36,** 55–64, 2005.

[8] D. D. R. Cartié, M. Troulis, I. K. Partridge, Delamination of Z-pinned carbon fibre reinforced laminates. *Composites Science and Technology,* **66**, 855–861, 2006.

[9] C. A. Steeves, N. A. Fleck, In-plane properties of composite laminates with through-thickness pin reinforcement. *International Journal of Solids and Structures*, **43** 3197–3212, 2006.

[10] P. Chang, A. P. Mouritz, B. N. Cox, Properties and failure mechanisms of z-pinned laminates in monotonic and cyclic tension. *Composites: Part A* **37**, 1501–1513, 2006.

[11] D. D. R. Cartie, G. Dell'Anno, E. Poulin, I. K. Partridge, 3D reinforcement of stiffener-to-skin T-joints by Z-pinning and tufting. *Engineering Fracture Mechanics,* **73,** 2532–2540, 2006.

[12] G. Dell'Anno, D. D. R. Cartié, I. K Partridge, A. Rezai. Exploring mechanical property balance in tufted carbon fabric/epoxy composites. *Composites Part A: Applied Science and Manufacturing*, article in press available online 5 July, 2007.

[13] Standard test methods for mode I interlaminar fracture toughness of unidirectional fiber reinforced polymer matrix composites. Designation: D5528-01, *Annual book of ASTM Standards*, **15.03,** 2004

[14] A. B. Pereira, A. B. de Morais, Mode I interlaminar fracture of carbon/epoxy multidirectional laminate. Composites Science and Technology, **64,** 2261–2270, 2004.

[15] A. J. Brunner, B. R. K. Blackman and P. Davies, A status report on delamination resistance testing of polymer–matrix composites. *Engineering Fracture Mechanics*, 2007.

[16] PAM-CRASH^{TM} *Users manuals, Engineering Systems International*. 20 Rue Saarinen, Silic 270, 94578 Rungis-Cedex, France. Available from: www.esi-group.com, 2006.

[17] A. F. Johnson, A. K. Pickett, P. Rozycki, Computational methods for predicting impact damage in composite structures. *Composites Science and Technology*, **61**, 2183–2192, 2001.

[18] L. Greve , A. K. Pickett, Delamination testing and modelling for composite crash simulation. *Composites Science and Technology,* **66,** 816–826, 2006.

[19] L. Greve and A. K. Pickett, Modelling damage and failure in carbon/epoxy non-crimp fabric composites including effects of fabric pre-shear. *Composites Part A: Applied Science and Manufacturing*, **37**, Pages 1983-2001, 2006.

[20] P. Ladeveze, E. Le Dantec Damage modelling of the elementary ply for laminated composites. *Composites Science and Technology,* **43,** 257–67, 1992.